

The Berrettini palmar neural communicating branch: a study of 27 cadaveric specimens and determination of a high-risk surgical zone

Akos Marton¹ , Shahzaib Ahmed¹, Gavin E. Jarvis², Cecilia Brassett¹, Ian Grant^{1,3} and Michael E. Gaunt¹

Journal of Hand Surgery
(European Volume)
0(0) 1–6
© The Author(s) 2022



Article reuse guidelines:
sagepub.com/journals-permissions
DOI: 10.1177/17531934221095401
journals.sagepub.com/home/jhs



Abstract

In this cadaveric study, we analysed digital images of dissected palms to define the location and length of superficial connections between the median and the ulnar nerves (Berrettini communicating branches). We found the connections present in 12 of 27 hands. We used a coordinate model to define their location relative to seven specified landmarks. The model revealed that the Berrettini communicating branches were positioned consistently, and we defined a high-risk zone in the palm that fully contained seven of the 12 connections, while others had minor projections outside the zone. We conclude that awareness of this high-risk zone in the palm can be of some help to reduce the risk of iatrogenic nerve injury, however, any operation in the palm must always be done with great care to visualize and protect any possible anatomically unusual structures.

Keywords

Anatomical study, median nerve, ulnar nerve, Berrettini anastomosis

Date received: 12th October 2021; revised: 21st March 2022; accepted: 3rd April 2022

Introduction

Communicating branches between the major nerves in the hand are a potential cause of clinical and neurophysiological misdiagnosis and a site of injury during hand surgery. The Berrettini communicating branch (BCB) is an ulnar-to-median sensory nerve connection with a reported prevalence of 60% (Roy et al., 2016). With its superficial position and close relation with the flexor retinaculum, it is particularly vulnerable to iatrogenic injury (Roy et al., 2016) (Figure 1(a) and (b)). While the BCB is usually clinically silent, it may be associated with atypical patterns of sensory innervation leading to a complex neurological assessment and unexpected patterns of sensory disturbance (Seidel et al., 2020; Stopford, 1918). A recent meta-analysis highlighted a wide variance of data in reported prevalence of this communicating branch, possibly due to different study methodologies and reporting parameters. This led to recommended standardized reporting standards for future studies (Roy et al., 2016).

Computer-based modelling of high-quality digital images can facilitate detailed anatomical investigation and analysis. In this cadaveric study, we report the prevalence, length and angle of the BCB, and employ digital image analysis technology, coordinate data transformation and statistical modelling to define quantitatively the anatomy of the BCB and establish a high-risk dissection zone that best reflects the likely location of the BCB.

¹Department of Physiology, Development and Neuroscience, University of Cambridge, Cambridge, UK

²School of Medicine, University of Sunderland, Sunderland, UK

³Department of Plastic and Reconstructive Surgery, Addenbrooke's Hospital, Cambridge, UK

Corresponding Author:

Akos Marton, Human Anatomy Centre, Department of Physiology, Development and Neuroscience, University of Cambridge, Downing Site, Cambridge CB2 3DY, UK.

Email: am2485@cam.ac.uk; akosmarton97@gmail.com

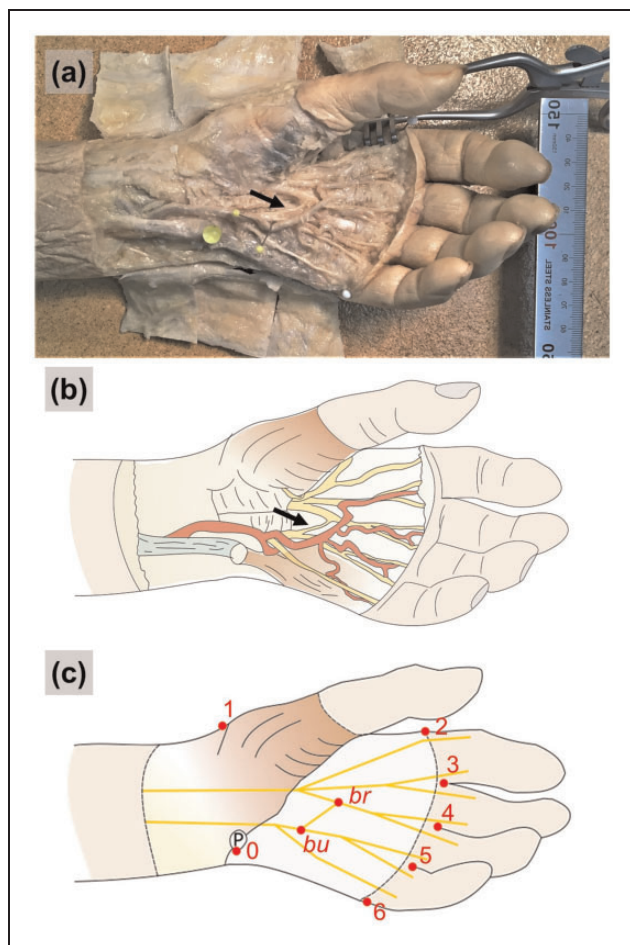


Figure 1. (a) Specimen No. 6 with the Berrettini communicating branch present (arrow). (b) Schematic drawing showing the anatomy of the same specimen. (c) Schematic drawing showing the landmarks measured using ImageJ. Landmarks – 0: ulnar border of pisiform bone; 1: radial border of wrist; 2: base of the index finger at the level of palmar digital crease; 3: midpoint of skin margin in second web space; 4: midpoint of skin margin in third web space; 5: midpoint of skin margin in fourth web space; 6: ulnar border of the little finger at the level of palmar digital crease; bu: ulnar endpoint of Berrettini communicating branch; br: radial endpoint of Berrettini communicating branch; P: pisiform bone.

Methods

Specimens

Twenty-seven cadaver hands were embalmed using a 4.2% formaldehyde solution. One hand from each donor was selected for dissection, giving a sample of 13 right and 14 left hands. Donors were from the catchment area of the University of Cambridge, England, UK, as defined by the Human Tissue Authority (<https://www.hta.gov.uk/medical-schools>), and all had provided written consent to the use of

their bodies in anatomical research. (Donor information is found in Supplementary Table S1.)

Dissection and measurements

Superficial dissection of the palm was performed to achieve unrestricted access to the branches of the ulnar and median nerves. After skin removal, the relevant neurovascular structures were dissected and identified. A communicating branch between two nerves was identified as a BCB if the two endpoints were superficial palmar branches of the ulnar and median nerves (Figure 1). In those hands, in which a BCB was identified, high-quality digital photographs were taken. In each case, a ruler, elevated to level of the palmar plane, was in the frame to aid subsequent calibration. The length and angle (defined as the angle between the common digital nerve from which it arises and the BCB branch) were measured from the digital photographs using ImageJ image analysis software (v.1.52a, National Institutes of Health, Bethesda, MD, USA). ImageJ was calibrated to convert pixels to millimetres using the in-frame ruler.

Constructing a coordinate model

A coordinate model of the hand was constructed to define the location of the BCB within the palm using the digital images. The X dimension was from proximal to distal, and the Y dimension from ulnar to radial. The pisiform was defined as the origin (0,0, landmark 0) and the coordinate values were in millimetres. X , Y coordinates for the two endpoints of the BCB on ulnar (*bu*) and radial (*br*) sides, and that of seven fixed landmarks (0 to 6) defining the hand perimeter were obtained from each hand (Figure 1(c)). These were the raw coordinates (X_{raw} , Y_{raw}). Landmarks 0 to 6 were defined as:

- 0: Ulnar border of pisiform bone
- 1: Radial border of wrist
- 2: Base of the index finger at the level of palmar digital crease
- 3: Midpoint of skin margin in second web space
- 4: Midpoint of skin margin in third web space
- 5: Midpoint of skin margin in fourth web space
- 6: Ulnar border of the little finger at the level of palmar digital crease

Superimposition of the raw coordinates did not result in an optimized inter-subject anatomical comparison (Supplementary Figure S1a). To eliminate the inter-subject differences in size and rotation in the digital photographs, and thus achieve an optimized model, raw coordinates were subject to three

transformations ensuring the original anatomical proportions of each hand were preserved.

The transformations were performed as follows (photographs of left hands were used as they were, while photographs of right hands were mirrored, and all the coordinates were treated as if from left hands).

1. For each hand, the mean of the X and Y coordinates for the seven anatomical landmarks ($\bar{x}_{l,raw}$ and $\bar{y}_{l,raw}$), were subtracted from each of the seven fixed and two BCB landmarks to generate a new set of nine coordinates (termed: X_{t1}, Y_{t1}). This has the effect of shifting the origin from the pisiform (landmark 0) to a location in the centre of the palm, such that $\bar{x}_{lt1} = \bar{y}_{lt1} = 0$. This transformation was independent in each hand and the resulting coordinates are shown in Supplementary Figure S1b.
2. The X_{t1}, Y_{t1} coordinates in each hand were subject to a rotational transformation centred on the origin ($\bar{x}_{lt1}, \bar{y}_{lt1}$) using a rotation matrix such that:

$$\begin{bmatrix} X_{t2} \\ Y_{t2} \end{bmatrix} = \begin{bmatrix} \cos \theta & -\sin \theta \\ \sin \theta & \cos \theta \end{bmatrix} \begin{bmatrix} X_{t1} \\ Y_{t1} \end{bmatrix}$$

where θ is a variable parameter equal to the anti-clockwise rotational angle, and was constant within a hand but varied between hands. The effect of this transformation was to rotate the images of the hands so that they were aligned as closely as possible, as defined by the objective function (see below). The resulting coordinates are shown in Supplementary Figure S1c.

3. The X_{t2}, Y_{t2} coordinates in each hand were subject to a scalar transformation of the form:

$$\begin{bmatrix} X_{t3} \\ Y_{t3} \end{bmatrix} = S \begin{bmatrix} X_{t2} \\ Y_{t2} \end{bmatrix}$$

where S is a variable parameter equal to the uni-dimensional fold change brought about by the transformation. It is constant within a hand and varies between hands. The effect of this transformation was to scale the images of the hands up or down so that they were aligned as closely as possible, as defined by the objective function (see below). The resulting coordinates are shown in Supplementary Figure S1d.

Unique values of θ and S were estimated for each hand such that $\bar{\theta} = 0$, and $\bar{S} = 1$, meaning that across all hands there was no net rotation and no net

change in scale. $N - 1$ values of θ and of S were estimated: the remaining non-estimated value of θ was constrained to equal the negative sum of the 11 estimated θ 's, and the non-estimated value of S was constrained to equal 12 minus the sum of the estimated 11 S 's.

Estimates of the parameters θ and S were obtained by minimizing an objective function (OBJ). This was the sum across all hands ($n=12$) of the squared deviations from the mean for the seven paired landmark coordinates ($X_{l,t3}, Y_{l,t3}$) within each hand as:

$$OBJ = \sum_{j=1}^{12} \left(\sum_{i=0}^6 (x_{i,t3} - \bar{x}_{l,t3})^2 + \sum_{i=0}^6 (y_{i,t3} - \bar{y}_{l,t3})^2 \right)$$

where j indicates each hand and i indicates each fixed anatomical landmark.

Minimization was performed using the Solver function in Microsoft Excel. Post-minimization, $OBJ=773.0$, and the estimates of the parameters for each hand are shown in Supplementary Table S2. In effect, the transformations generated a coordinate map for a rotationally and size-standardized hand. The coordinate values (mean, SD) for the seven landmarks are illustrated in Supplementary Figure S1.

For each hand, using the values in Supplementary Table S2, the three transformations were applied to the raw BCB coordinates to obtain new coordinates that mapped onto the standardized hand. The resulting coordinates were: $\bar{x}_{bu,t3} = -35.1$ SD 6.8 $\bar{y}_{bu,t3} = -9.6$ SD 3.3 and $\bar{x}_{br,t3} = -19.9$ SD 6.1 $\bar{y}_{br,t3} = -0.5$ SD 2.8. Supplementary Figure S1d shows the final model.

The transformations resulted in a graphical model that shows the defined anatomical landmarks and BCBs from each hand superimposed and readily comparable (Figure 2). This model was used to identify a high-risk dissection zone in the palm. Potential definitions of such a zone based on the defined anatomical landmarks were assessed and the number of BCB endpoints within proposed zones compared. Each zone was defined by four points: two points along the line between landmarks '0' and '2', and two points along the line between landmarks '0' and '4' (Figure 1(c)). The location of the four points along the lines ranged from 0% to 100% of total distance, in 5% increments. The number of anatomical endpoints – of a total of 24 endpoints from 12 BCBs – contained within each of the potential zones were assessed to identify the most comprehensive and anatomically minimized definition of the high-risk zone (Supplementary Figure S2a-b).

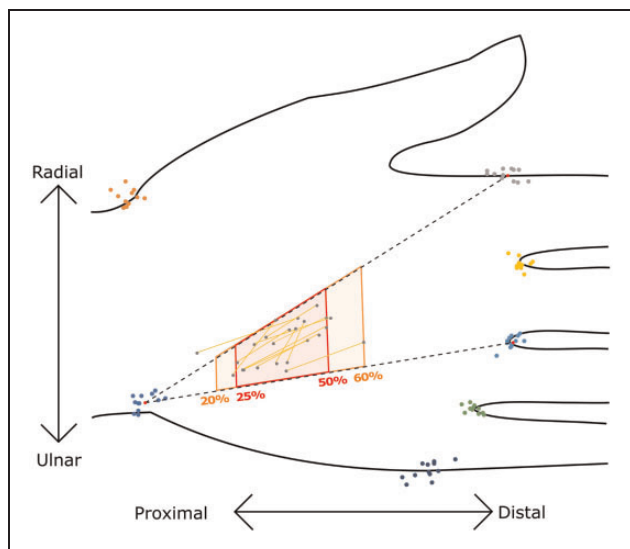


Figure 2. The hand model after the transformations. The landmarks and the Berrettini communications from the 12 hands with a communicating branch are shown. The zones according to the 25% to 50% and the 20% to 60% definitions are shown.

Statistics

Length and angle values are shown with standard deviation (SD) estimates throughout. Associations between the presence of a BCB and either sex or side were evaluated using Fisher's exact test. Two-tailed p -values are reported. The level of significance was set at $p < 0.05$.

Results

The BCB was identified in 12 of 27 hands, being present in 6/13 male specimens and 6/14 female specimens ($p=1.0$). More BCBs were found in right (9/13) compared with left (3/14) hands ($p=0.021$) (Supplementary Table S1). The mean length of the BCB was 20 mm (SD 5, range 10–31 mm). The mean angle between the communicating branch and the nerve trunk of origin was 29° (SD 15, range 17° – 61°) (Supplementary Table S3). We observed two cases where the BCBs enclosed angles larger than 45° : 54° (Specimen no. 7) and 61° (Specimen no. 12).

The graphical model from the coordinate data transformation showed clustering of the BCBs in a small region of the palm. We assessed 231 potential zones to define a high-risk dissection zone that best reflects the location of the BCBs (Supplementary Figure S2). The most inclusive yet smallest high-risk zone was the area between the four points at 20% and 60% of total distance along the lines

between landmarks '0' and '2' or '4' (Figure 2). This contained 22/24 endpoints of the 12 BCBs.

A clinically more easily adoptable version of the high-risk 'danger' dissection zone was defined using 25% and 50% of the total distance along the two lines (Figure 2). In the model, this contained 19/24 endpoints of the 12 BCBs and 8/12 full-length BCBs. This danger zone can be found using the following steps.

1. Locate the ulnar border of the pisiform.
2. Draw a line from the ulnar border of the pisiform to the radial border of the base of the index finger at the level of the palmar digital crease. Mark the halfway point along that line, then the halfway point along the proximal half-segment.
3. Draw another line from the ulnar border of the pisiform to the skin margin in the third web space between the middle and ring fingers. Mark the halfway point along this line, then the halfway point along the proximal half-segment.
4. The quadrilateral defined by these four marked points outlines the danger zone where the BCB is likely to be located if present.

This 25% to 50% procedure was applied to each photograph of the 12 hands, thereby mimicking a pre-surgical evaluation in an individual patient. In 7/12 hands the BCB lay fully within the danger zone, and 18/24 endpoints were within the same zone with minimal projection beyond the border of the zone.

Discussion

This study investigated the anatomy of the BCB within a convenience sample of cadavers drawn from a geographical area surrounding Cambridge, UK, and focused on its prevalence and location in the palm. We confirmed that the BCB is a common variant, and our statistical modelling enabled us to define an easily identifiable zone where the BCB is likely to be located, if present.

The prevalence in our sample (12/27 hands) was in the lower mid-range of reported prevalence in the literature. The average reported in the literature is 61%, with marked variability in the results of other authors, ranging from 4% to 96% (Bas and Kleinert, 1999; Don Griot et al., 2000; Ferrari and Gilbert, 1991; Hoogbergen and Kauer, 1992; Loukas et al., 2007; Meals and Shaner, 1983; Olave et al., 2001; Roy et al., 2016; Stančić et al., 1999; Sulaiman et al., 2016; Tagil et al., 2007; Zolin et al., 2014). This wide range may be caused by a variety of reasons related to differing methods of dissection and reporting

standards. The high occurrence of BCB in the hand observed here and by other authors suggests that this communicating branch is not a rare anatomical variant and may be considered more of a normal mingling of the fibres of the ulnar and median nerves.

Roy et al. (2016) recommended a standardized classification system for future studies, comprising three types of BCBs based on their transverse orientation. In the current study, all BCBs were in an ulnar to median orientation. The mean length was 20 mm (SD 5.5), consistent with reports in the literature. The meta-analysis by Roy et al. (2016) reported a mean length of 19 mm (SD 8.7) in 63 upper limbs. The mean angle between the communication and its nerve branch of origin was 29° (SD 15). Communicating branches that course at a close-to-perpendicular angle have been proposed to be at higher risk of being severed during surgery (Ferrari and Gilbert, 1991). Procedures with the greatest risk of iatrogenic injury include open and endoscopic carpal tunnel release, ring finger flexor tendon surgery, Dupuytren's fasciectomy and mobilization of neurovascular island flaps (Loukas et al., 2007).

A well-defined danger zone may assist surgeons in estimating where a communicating branch may lie. Previous descriptions of such a region were defined with reference to variable soft tissue surface landmarks, such as wrist and palmar creases (Ferrari and Gilbert, 1991; Loukas et al., 2007; Sulaiman et al., 2016), or to deep bony landmarks that are not always easily identifiable, such as the styloid processes of the ulnar and radial bones and the metacarpophalangeal joints (Don Griot et al., 2000).

We defined a high-risk zone for dissection in terms of distances along the lines from the pisiform to the bases of the index and ring fingers. A large set of potential definitions of this zone were assessed. When assessing how many endpoints were contained in each of these potential zones, we found that the smallest yet most inclusive definition of the high-risk zone was at 20% and 60% of the total distances along both lines, which contained 22 of 24 endpoints of the 12 BCBs. In addition to the 'optimal' 20%–60% high-risk zone, we defined a 25%–50% danger zone, which in our clinical judgement is easier to adopt in practice, containing seven BCBs completely and the majority of the length of the remaining five BCBs within the zone. Our proposed definition of the danger zone has two advantages over previous ones. First, it is defined in terms of standardized distances measured from the ulnar vertex of the pisiform, which is an easily palpable bony landmark and constant reference point. Second, it was defined using a quantitative approach that simplifies considerably the illustration of this anatomical variant and

provides a method for reproducible numerical analysis. We propose this method may be used to report anatomical variation in future studies.

This study has some limitations. The sample size was small, with 27 hands dissected in total, and the BCB identified in 12 of these. Such a small sample, in conjunction with the inherently variable anatomy of the BCB, will limit the gravity of the above results when translated into clinical practice. Furthermore, the number of BCBs that lie partly outside of the proposed danger zone is not insignificant. While the proposed high-risk dissection zone can provide rough guidance, it is not intended to be a definitive representation of where the BCB is located, and dissection in the palm must always be done with great care to identify and protect possible anatomic variations such as the BCB.

Acknowledgements The authors would like to express their sincerest gratitude to the donors without whose generous gift this project could not have been possible. We would like to acknowledge the help and support of Maria Wright, James Skeates and Darren Broadhurst, dissection room staff of the Human Anatomy Centre, University of Cambridge.

Declaration of conflicting interests The authors declare no potential conflicts of interest with respect to the research, authorship, and/or publication of this article.

Funding The authors disclosed receipt of the following financial support for the research, authorship, and/or publication of this article: this work was funded by the University of Cambridge.

Ethical approval declaration Ethical approval was not sought for the present study.

Informed consent declaration Written consent was obtained from all donors before decease for the use of their bodies for anatomical research, in compliance with the Human Tissue Act (2004).

ORCID iD Akos Marton  <https://orcid.org/0000-0002-3974-1178>

Supplemental material Supplemental material for this article is available online.

References

- Bas H, Kleinert JM. Anatomic variations in sensory innervation of the hand and digits. *J Hand Surg Am.* 1999, 24: 1171–84.
- Don Griot JPW, Zuidam JM, Van Kooten EO, Prosé LP, Hage JJ. Anatomic study of the ramus communicans between the ulnar and median nerves. *J Hand Surg Am.* 2000, 25: 948–54.

- Ferrari GP, Gilbert A. The superficial anastomosis on the palm of the hand between the ulnar and median nerves. *J Hand Surg Am.* 1991, 16: 511–4.
- Hoogbergen MM, Kauer JMG. An unusual ulnar nerve-median nerve communicating branch. *J Anat.* 1992, 181: 513–6.
- Loukas M, Louis RG, Stewart L et al. The surgical anatomy of ulnar and median nerve communications in the palmar surface of the hand. *J Neurosurg.* 2007, 106: 887–93.
- Meals RA, Shaner M. Variations in digital sensory patterns: a study of the ulnar nerve—median nerve palmar communicating branch. *J Hand Surg Am.* 1983, 8: 411–4.
- Olave E, Del Sol M, Gabrielli C, Mandiola E, Rodrigues CFS. Biometric study of the relationships between palmar neurovascular structures, the flexor retinaculum and the distal wrist crease. *J Anat.* 2001, 198: 737–41.
- Roy J, Henry BM, Pękala PA et al. Median and ulnar nerve anastomoses in the upper limb: a meta-analysis. *Muscle and Nerve.* 2016, 54: 36–47.
- Seidel GK, Seidel ME, Hakopian D et al. Frequency of electrodiagnostically measurable Berrettini anastomosis. *J Clin Neurophysiol.* 2020, 37: 214–9.
- Stančić MF, Mićović V, Potočnjak M. The anatomy of the Berrettini branch: implications for carpal tunnel release. *J Neurosurg.* 1999, 91: 1027–30.
- Stopford JS. The variation in distribution of the cutaneous nerves of the hand and digits. *J Anat.* 1918, 53: 14–25.
- Sulaiman S, Soames R, Lamb C. An anatomical study of the superficial palmar communicating branch between the median and ulnar nerves. *J Hand Surg Eur.* 2016, 41: 191–7.
- Tagil SM, Bozkurt MC, Özçakar L, Ersoy M, Tekdemir I, Elhan A. Superficial palmar communications between the ulnar and median nerves in Turkish cadavers. *Clin Anat.* 2007, 20: 795–8.
- Zolin SD, Barros MD, Abdouni YA, Nascimento VDG, Costa AC Da, Chakkour I. Anatomical study of sensory anastomoses in the hand. *Acta Ortop Bras.* 2014, 22: 34–7.